Analytical and Bioanalytical Chemistry (2022) 414:7191–7201
https://doi.org/10.1007/s00216-022-04271-5

RESEARCH PAPER

Mesoporous platinum nanoparticles as a peroxidase mimic for the highly sensitive determination of C-reactive protein

Seong Eun Son[1] · Pramod K. Gupta[1] · Won Hur[1] · Han Been Lee[1] · Yosep Park[1] · Jiyeon Park[1] · Seong Nyeon Kim[1] · Gi Hun Seong[1]

Received: 26 May 2022 / Revised: 18 July 2022 / Accepted: 8 August 2022 / Published online: 15 August 2022

Abstract

The generation of a mesoporous structure in platinum nanoparticles can effectively enhance physical and chemical properties. In this study, mesoporous platinum nanoparticles (MPNs) were synthesized by a soft template-mediated one-pot chemical method. To develop a mesoporous structure, Pluronic F-127 was employed. The Pluronic F-127 surfactant forms self-assembled micelles, and the micelles act as the pore-directing agents in the synthesis of nanoparticles. Scanning electron microscopy results revealed that the MPN had a uniform size of 70 nm on average and a distinct mesoporous structure. The development of a concave mesoporous structure on the surface of the MPNs can increase the surface area and facilitate the efficient transport of reactants. The synthesized MPNs exhibited peroxidase-like activity. Furthermore, the MPNs showed excellent catalytic efficiency compared to HRP, due to the high surface area derived from the presence of the mesoporous structure. The peroxidase-like MPNs were applied to the enzyme-linked immunosorbent assay (ELISA) of C-reactive protein (CRP). The MPN-based ELISA exhibited sensitive CRP detection in the range from 0.24 to 7.8 ng/mL with a detection limit of 0.13 ng/mL. Moreover, the recoveries of the CRP concentrations in spiked human serum were 98.6% and 102%. These results demonstrate that as a peroxidase mimic, the MPNs can replace the natural enzymes in conventional ELISA for sensitive CRP detection.

Keywords Mesoporous nanoparticle · Nanozyme · Colorimetric detection · C-Reactive protein · Enzyme-linked immunosorbent assay

Introduction

In recent years, nanozymes, the nanomaterials which show the enzyme-like activity, have been considered as substitutes to natural enzymes due to significant advantages, such as their ease of preparation and storage, high stability, and great catalytic activity [1]. Since magnetite nanoparticles were identified as a peroxidase mimic [2], a variety of nanomaterials, such as metal–organic frameworks, carbon-based materials, metal oxides, and noble metals, have shown enzyme-like activities [3–9]. Among these nanomaterials, platinum (Pt)-based nanomaterials showed great catalytic activities with excellent sensitivity and good stability. Therefore, Pt-based nanomaterials are considered promising catalysts for biomedical applications such as immunoassays, biomolecule detection, and other applications. To date, various Pt-based nanomaterials showed several enzyme mimicking activities such as catalase, peroxidase, and oxidase [10–14]. Although various Pt-based nanomaterials have been developed and show enzyme-like activities, the utilization of these nanomaterials as enzyme mimics remains unexplored due to challenges in controlling the surface properties, morphology, and size to enhance the enzyme-like activities.

Recently, the development of mesoporous nanoparticles has attracted attention due to the presence of small-sized pores, which allows the facile transfer of reactants [15]. In mesoporous structures, abundant active sites are exposed due to the high surface area. The mesoporous architectures can be synthesized using various methods, including electrochemical deposition, galvanic replacement, and soft or hard template-mediated synthesis [16–19]. Of these several methods, soft template and chemical reduction mediated

✉ Gi Hun Seong
ghseong@hanyang.ac.kr

[1] Department of Bionano Engineering, Center for Bionano Intelligence Education and Research, Hanyang University, Ansan 426-791, South Korea

approaches have significant advantages, such as simple synthetic steps, ease of template removal, and good repeatability [20]. In recent years, various mesoporous noble metal nanomaterials (e.g., Rh, Pd, and Pt) were synthesized using micelles as a pore-directing template. These mesoporous nanomaterials showed enhanced catalytic activities in various applications, such as electrochemical methanol oxidation and ethanol oxidation [21–23]. However, as far as we know, the application of mesoporous noble metal nanoparticles as enzyme mimics has not been studied.

C-reactive protein (CRP) is an important indicator of the inflammatory response in the acute phase produced principally by the liver and found in human plasma [24]. Moreover, high-sensitivity CRP levels in the blood are associated with cardiovascular disease [25]. Therefore, it is important to monitor the CRP level in patients for the diagnosis of lethal diseases. As a conventional method, the enzyme-linked immunosorbent assay (ELISA) has been employed in clinical applications for quantifying the CRP level. In ELISA, the critical parameter is the enzyme activity. Typically, ELISA employs natural enzymes, such as horseradish peroxidase (HRP), which catalyzes the oxidation of organic substrates in the presence of hydrogen peroxide (H_2O_2). Although natural enzymes exhibit high catalytic efficiency, these enzymes have several disadvantages including complex preparation, high cost, and denaturation under harsh environments. Consequently, the use of nanomaterials with enzyme-like activity can be an excellent way to overcome the disadvantages of natural enzymes.

In this study, we fabricated mesoporous Pt nanoparticles (MPNs) by a simple soft template-mediated synthetic method. The enzyme-like activity of the MPNs was evaluated by measuring the absorbance of 3,3′,5,5′-tetramethylbenzidine (TMB). The MPNs exhibited intrinsic peroxidase-like activity and quickly oxidized the TMB in the presence of H_2O_2 due to the high surface to volume ratio derived from the mesoporous structure. Then, the MPNs were applied to ELISA for CRP detection. The MPN-based ELISA exhibited a good linear relationship with the CRP concentration. Moreover, the MPN-based ELISA showed a higher sensitivity than conventional HRP-based ELISA in the same CRP concentration range. These results validate the possibility of MPNs as an effective alternative to natural enzymes for sensitive CRP detection.

Experimental section

Materials

Pluronic F-127, potassium bromide (KBr), L-ascorbic acid (AA), chloroplatinic acid hexahydrate ($H_2PtCl_6{\cdot}6H_2O$), uric acid, urea, glucose, creatinine, 5,5′-dithiobis (2-nitrobenzoic acid) (Ellman's reagent), N-(3-dimethylaminopropyl)-N′-ethylcarbodiimide hydrochloride (EDC), bovine serum albumin (BSA), human serum albumin, ethylenediaminetetraacetic acid (EDTA), N-hydroxysulfosuccinimide (sulfo-NHS), TMB, phosphate buffer (1.0 M, pH 7.4), poly(ethylene glycol) 2-mercaptoethyl ether acetic acid ($HS\text{-}PEG_{3500}\text{-}COOH$, MW ≈ 3500), terephthalic acid (TA), hydrogen peroxide (H_2O_2), dimethyl sulfoxide (DMSO), and sodium acetate (NaAc) were purchased from Sigma-Aldrich (St. Louis, MO, USA). Acetic acid (HAc) was obtained from Junsei Chemical Co., Ltd. (Tokyo, Japan). Sulfuric acid (H_2SO_4, 98%) was purchased from Daejung Co., Ltd. (Siheung, South Korea). Indium tin oxide (ITO) glass was supplied from Samsung Corning Advanced Glass (Asan, South Korea). 20X phosphate-buffered saline (PBS, pH 7.4) was acquired from Biosesang Co., Ltd. (Seongnam, South Korea). The laminating film was purchased from Two-Hand Co., Ltd. (Anseong, South Korea). The mouse anti-CRP monoclonal capture and detection antibodies (cAb-CRP and dAb-CRP) were obtained from Fitzgerald Industries International (Acton, MA, USA).

Synthesis of MPNs

The MPNs were synthesized by modifying a previously reported method [26]. Briefly, 150 mg of KBr and 30 mg of Pluronic F-127 were added to 2 mL of DI water. The solution was sonicated to completely dissolve the KBr and Pluronic F-127. Then, 0.75 mL of a $H_2PtCl_6{\cdot}6H_2O$ solution (40 mM) was added and incubated for 5 min under gentle shaking. At this point, the color of the solution changed from bright yellow to orange. Finally, 2 mL of an AA solution (100 mM) was added. The solution was incubated in an oil bath for 12 h at 70 °C. The sample was washed by four consecutive cycles using ethanol and water. Finally, the pure MPNs were resuspended in 4 mL of water and stored at 4 °C.

Enzyme-like activity of the MPNs

The enzyme-like activity of the MPNs was investigated by using the reaction between TMB and H_2O_2. In the reaction, TMB and H_2O_2 were introduced to 0.1 M HAc-NaAc buffer (pH 5.5) that contains the MPNs (0.5 μg/mL). Then, the time-dependent absorbance of the mixed solution was measured at a wavelength of 652 nm. To evaluate the catalytic efficiency, the Michaelis constant (K_m) and maximum reaction rate (V_{max}) were determined using the Lineweaver–Burk equation, which was derived from the double-reciprocal of the Michaelis–Menten equation. Moreover, the turnover number (K_{cat}) was calculated by dividing V_{max} by the nanozyme concentration. The detailed equations are depicted in the Supplementary Information.

Evaluation of the catalytic system of the MPNs

To verify the production of hydroxyl radicals (•OH) from H_2O_2 decomposition by the MPNs, TA was employed. In brief, the 0.5 mM TA, 20 mM H_2O_2, and 1.0 μg/mL MPNs were mixed. After 50 min incubation at room temperature, the fluorescence was recorded with an excitation wavelength of 315 nm.

The electrochemical experiments were conducted to investigate the electron transfer between the MPNs and substrates. The ITO glass was modified with the MPNs and Nafion and used as a working electrode. Briefly, 10 μL of MPNs (10 μg/mL) was dropped onto ITO glass and dried, followed by the addition of 10 μL of 0.5% Nafion. Finally, the modified ITO electrode (Nafion/MPN/ITO) was washed using water and dried. As a reference and counter electrode, the Ag/AgCl (saturated in 3 M NaCl) and a platinum wire were used, respectively. In electrochemical experiments, all three electrodes were placed in 5 mL PBS (10 mM). In cyclic voltammetry, the current value was monitored at room temperature and potential range of −1.0–0 V. In chronoamperometry analysis, the current response was monitored by adding 50 μL of 1 M H_2O_2 to the PBS solution every 50 s under continuous stirring.

PEGylation of MPNs

To introduce carboxyl groups, the MPNs were conjugated with HS-PEG_{3500}-COOH. First, 330 μL of 50 μM HS-PEG_{3500}-COOH was mixed with the same amount of a 5 mg/mL MPN solution. The mixed solution was incubated for 4 h at room temperature. Then, the solution was centrifuged to precipitate the PEG-modified MPNs (MPN-S-PEG_{3500}-COOH). The supernatant was carefully separated and stored. The MPN-S-PEG_{3500}-COOH precipitates were washed twice with DI water. Finally, the MPN-S-PEG_{3500}-COOH was redispersed in 660 μL of DI water.

The PEGylation of MPNs was confirmed by Ellman's test. The thiol groups of HS-PEG_{3500}-COOH can react with the Ellman's reagent, generating a yellow-colored product. First, 100 μL of carefully separated supernatant was mixed with 150 μL of 0.3 M phosphate buffer containing 1 mM EDTA (pH 8.0). Then, 5 μL of Ellman's reagent dissolved in 0.5 M phosphate buffer containing 1 mM EDTA (pH 8.0) was added. After 10 min incubation at room temperature, the absorbance was recorded at a wavelength of 412 nm. 25 μM HS-PEG_{3500}-COOH was employed as a control to compare the absorbance signal of the supernatant.

Preparation of dAb-CRP/MPN conjugates

The mouse anti-CRP monoclonal detection antibody (dAb-CRP) conjugated MPN (dAb-CRP/MPN) was prepared by chemically modifying the MPN-S-PEG_{3500}-COOH with the dAb-CRP. Briefly, 5 μL of EDC (25 mM) and 5 μL of sulfo-NHS (25 mM) were mixed with 1 mL of MPN-S-PEG_{3500}-COOH (0.15 mg/mL). The solution was reacted for 1 h at room temperature. Then, the solution was washed two times with DI water and redispersed in 1 mL of DI water. Subsequently, 10 μL of dAb-CRP (1 mg/mL) was mixed with the solution. After incubation for 4 h at 4 °C, 110 μL of 2% BSA was added to block the unmodified surface of the MPNs. The solution was further incubated for 1 h at room temperature. Then, the dAb-CRP/MPN was purified two times with DI water. Finally, the dAb-CRP/MPN was redispersed in 0.5 mL of PBS (10 mM) containing 0.2% BSA.

Detection of CRP

To prepare the sandwich ELISA, the 96-well microplates were coated with mouse anti-CRP capture antibody (cAb-CRP). 100 μL of 5 μg/mL cAb-CRP dissolved in 50 mM carbonate/bicarbonate buffer (pH 9.6) was added to a microplate and incubated at 4 °C overnight. The microplates were washed three times with washing buffer (PBST, 10 mM PBS containing 0.05% Tween 20, pH 7.4). Then, 200 μL of 2% BSA dissolved in 100 mM PBS was added to block the microplates. After washing three times, the microplates were sealed and stored in a fridge until use.

Sandwich ELISA was performed for CRP detection. 100 μL of a CRP sample was added to cAb-CRP coated microplates and incubated for 2 h in a 37 °C oven. The microplates were washed three times with PBST and 100 μL of dAb-CRP/MPN (6 μg/mL in 10 mM PBS) was added. After incubation for 1 h at 37 °C, the microplates were washed five times with PBST. Then, 100 μL of the substrate solution (0.5 mM TMB and 50 mM H_2O_2 in 0.1 M HAc-NaAc, pH 5.5) was added. After incubation for 10 min at room temperature, 50 μL of H_2SO_4 (0.5 M) was added to stop the reaction. Then, the absorbance was recorded at a wavelength of 450 nm.

In the HRP-based ELISA, the procedure for the introduction of CRP to a microplate was the same as in the MPN-based ELISA. Then, 100 μL of HRP-anti-CRP antibody (0.5 μg/mL) was added and incubated for 1 h in a 37 °C oven. The microplate was washed three times using PBST. Then, 100 μL of the substrate solution (0.5 mM TMB and 5 mM H_2O_2 in 0.1 M HAc-NaAc buffer, pH 5.5) was added to each well. After incubation for 20 min, the reaction was stopped by the addition of 50 μL of 0.5 M H_2SO_4 and the absorbance was monitored at a wavelength of 450 nm.

Characterizations

The morphology and crystalline structure of the MPNs were confirmed using transmission electron microscopy (TEM,

JEOL JEM-2010, USA) and field-emission scanning electron microscopy (FE-SEM, Hitachi S-4800, Japan), and X-ray diffractometer (XRD, D/MAX-2500, Rigaku, USA), respectively. The absorbances were recorded using a UV–visible spectrometer (UV–vis, OPTIZEN 2120UV, Mecasys Co., Ltd., South Korea). All electrochemical experiments were performed using an electrochemical workstation (CHI 622C, CH Instrument Inc., USA) with a three-electrode system. A multi-mode microplate reader (BioTek Instrument Inc., USA) was utilized to monitor the absorbance.

Results and discussion

Characterization of MPNs

A schematic illustration of the simple micelle template-mediated synthesis of the MPNs is shown in Fig. 1. To synthesize the MPNs, Pluronic F-127 was employed as a pore-directing agent. The Pluronic F-127 forms a self-assembled micelle structure in which hydrophilic polyethylene oxide (PEO) faces outward and hydrophobic polypropylene oxide (PPO) faces inward. The generation of a micelle structure from the Pluronic F-127 was clearly indicated by the Tyndall effect. Above the critical micelle concentration (CMC) of 0.87 mg/mL [27], the micelle structures were generated from the self-assembly of Pluronic F-127. Then, the light was scattered due to the presence of colloidal micelles, showing a distinct line (Fig. S1A). However, the light scattering was not observed below the CMC (Fig. S1B). After micelle generation, the Pt precursor was stabilized by micelle through the interaction with ethylene oxide groups of the micelles [28]. Then, Pt clusters reduced by ascorbic acid continue to deposit on the surface of micelles, and the micelle-Pt nanoparticle complex was formed. Finally, the micelle was completely removed by consecutive washing, resulting in the generation of a mesoporous structure.

The crystalline structure of the MPNs was confirmed by XRD measurements (Fig. 2A). Four characteristic diffraction peaks corresponding to (111), (200), (220), and (311) planes were present in the XRD results, indicating a face-centered cubic (fcc) structure. The crystalline size, corresponding to the (111) plane of MPNs, was calculated to be 5.91 nm using Scherer's formula [29]. The morphology and structure of the MPNs were characterized by SEM (Fig. 2B). The SEM image indicates highly uniform and well-dispersed mesoporous structures with a diameter around 70 nm (inset of Fig. 2B). The size of the pores of the MPNs was around 14 nm (Fig. 2D). However, micrometer-sized Pt particles with a non-porous structure were obtained in the absence of micelle components, Pluronic F-127 (Fig. 2C). These results reveal the importance of Pluronic F-127 as a pore-directing agent to make the mesoporous structure. The mesoporous networks were also confirmed by TEM. The TEM images also display well-dispersed MPNs and obvious contrasts, demonstrating that the mesopores are embedded in the nanoparticles (Fig. 3A). However, the porous structure of the MPNs before washing the micelles was not clear (Fig. S2). Moreover, the high-angle annular dark-field scanning TEM (HAADF-STEM) image further evidences the presence of mesopores (Fig. 3B). Figure 3C displays a high-resolution TEM image of the MPNs. The lattice spacing at the surface of MPNs was 0.23 nm, which corresponds to the fcc Pt (111) plane. The selected-area electron diffraction (SAED) pattern of the MPNs exhibits distinct diffraction rings, suggesting a polycrystalline structure (Fig. 3D). Moreover, the four diffraction rings correspond to the (111), (200), (220), and (311) planes of the MPNs, which are consistent with the XRD results.

Enzyme-like activity of the MPNs

The enzyme-like activities of the MPNs were evaluated by monitoring the absorbance of TMB. The MPNs catalyzed

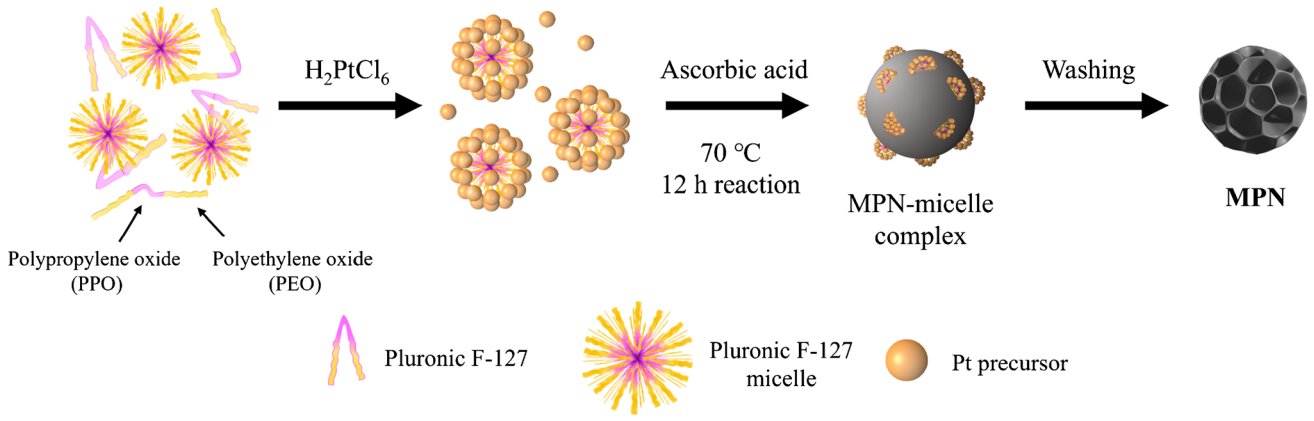

Fig. 1 Schematic diagram of the synthesis of the MPNs

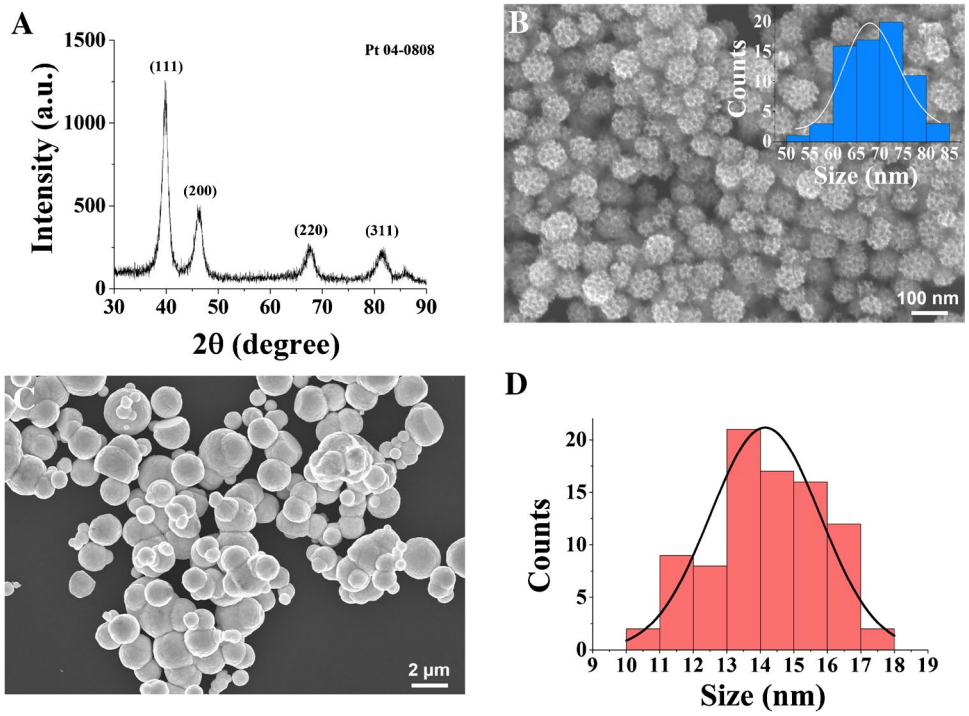

Fig. 2 **A** XRD result of the MPNs. SEM images of MPNs synthesized in the **B** presence and **C** absence of the Pluronic F-127. **D** Pore size distribution of the MPNs

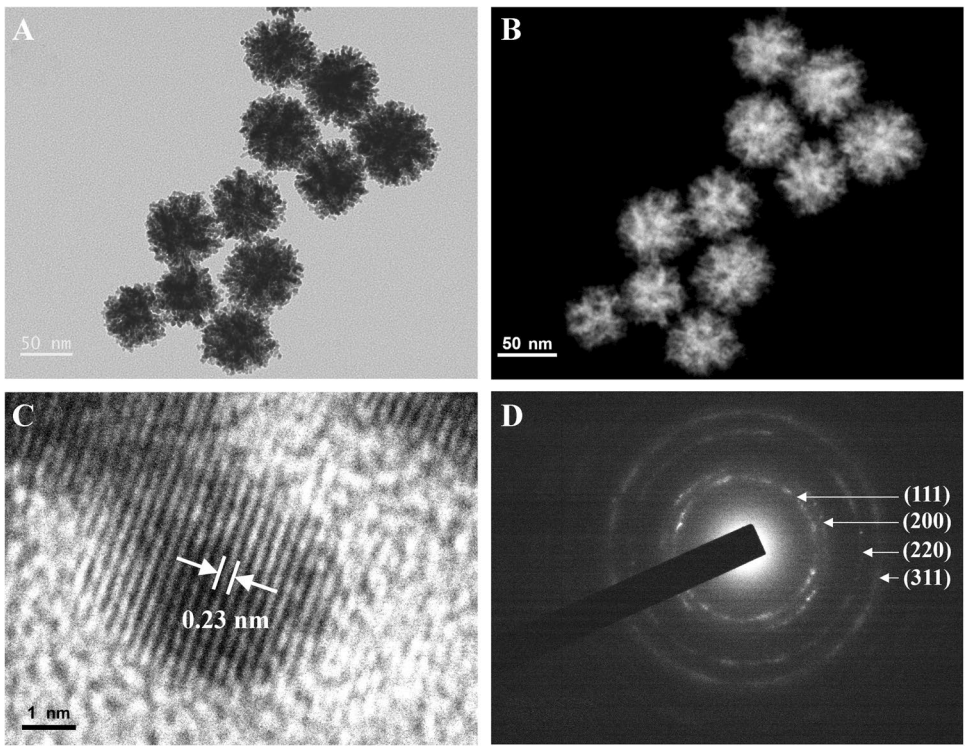

Fig. 3 **A** TEM and **B** HAADF-STEM images of the MPNs. **C** HR-TEM image of the MPNs. **D** SAED pattern of the MPNs

the oxidation of TMB and produced a blue-colored product (TMB_{ox}) in the presence of H_2O_2, suggesting peroxidase-like activity (Fig. 4). Moreover, the MPNs exhibit weak oxidase-like activity, which catalyzes the TMB oxidation in the absence of H_2O_2. However, this oxidase-like activity is negligible because it is considerably weaker than peroxidase-like activity.

Then, the optimal pH and temperature for the catalytic activity of the MPNs were studied. The maximum absorbance of TMB_{ox} was observed at pH 5.5, and it

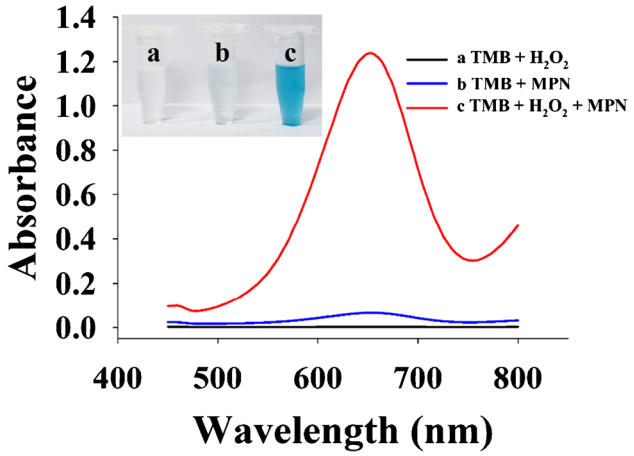

Fig. 4 UV–vis spectra displaying the enzyme-like activity of the MPNs. The inset displays photograph of TMB solutions with different compositions

decreased under lower or higher pHs (Fig. S3A). These results demonstrate that under weakly acidic conditions, the MPNs can catalyze the reaction of the TMB. Based on this result, the optimal temperature on the catalytic activity of MPNs was investigated at 4–60 °C at the optimized pH of 5.5. As shown in Fig. S3B, the maximum activity was observed from 15 to 30 °C. Above 30 °C, the activity decreased due to the invalid decomposition of H_2O_2 [30]. Thus, the temperature range of 15–30 °C was considered optimal. Based on these results, a pH of 5.5 and room temperature (25 °C) were adopted in the subsequent experiments.

The stabilities of the MPNs against various chemical and thermal conditions were explored. The MPNs were incubated at different pH (3.0–8.0) and temperature (25–70 °C). After 2 h incubation, the catalytic activity of MPNs was investigated by measuring the UV–vis absorbance of TMB_{ox}. HRP was also incubated at the same pH and temperature ranges for comparison. As shown in Fig. S4A, the MPNs show good stability under a broad range of pH values while HRP lost its stability under acidic conditions. In the case of temperature, the catalytic activity of the MPNs was stable under the range of temperature. However, the activity of HRP significantly decreased above 50 °C (Fig. S4B). These results reveal that the MPNs exhibit better stability for wide ranges of pH and temperature than HRP and can be used as a substitute for HRP. Then, the stability of the MPN solution for long-term storage at 4 °C was investigated over the course of a month (Fig. S4C). After a month, the catalytic activity of the MPNs was maintained at approximately 90%, which demonstrates good long-term stability of the MPNs.

Kinetic assay of MPNs

The catalytic activity and mechanism of the MPNs as a peroxidase mimic were investigated by evaluating the kinetic parameters of the reaction of TMB and H_2O_2. Figures 5A and D show the representative Michaelis–Menten curves of TMB and H_2O_2, respectively. The curves show the initial reaction velocity (V_0) as a function of the substrate concentration ([S]). As [S] increases, V_0 becomes saturated and reaches the maximum reaction velocity (V_{max}). The Michaelis–Menten curves were then converted to Lineweaver–Burk plots to determine the kinetic parameters of the MPNs including the Michaelis constant (K_m), V_{max}, and turnover number (K_{cat}) (Figs. 5B and E). The K_m value represents the enzyme's affinity to the substrates where the lower the K_m, the higher the affinity for the substrates. K_{cat} is the number of bound substrate molecules converted into a product by an enzyme per unit time. Thus, a higher K_{cat} corresponds to higher catalytic efficiency. These kinetic parameters of the MPNs were compared to other Pt-based nanoparticles and HRP (Table 1). The MPNs show a higher K_m value for TMB than other Pt-based catalysts and HRP, suggesting a lower affinity for TMB. In the case of H_2O_2, the MPNs also showed a lower affinity for H_2O_2 compared to the other catalysts. However, the K_{cat} values of MPNs for substrates are much higher than those of other catalysts and HRP. Especially, the K_{cat} values of the MPNs were higher than those of the Pd@Pt NPs, which were synthesized by the similar method. This result is due to the excellent peroxidase-like activity of Pt-based materials and the increased surface area by the mesoporous structure. These results suggest that the MPNs have the highest catalytic efficiency compared to other Pt-based nanomaterials and HRP. Figures 5C and F reveal the Lineweaver–Burk plots for different substrate concentrations. Parallel lines are displayed on each graph, suggesting that the reaction is based on the ping-pong mechanism. This mechanism was also observed in HRP [31]. These results demonstrate that the MPNs react with the first substrate and release the product before the reaction of the second substrate.

Catalytic mechanism of the MPNs

Although various peroxidase mimicking nanozymes have been developed, the obvious mechanisms of peroxidase-like nanozymes have not yet been revealed. One possible mechanism is the decomposition of H_2O_2 to hydroxyl radicals (•OH) by nanozymes. Then, •OH reacts with TMB, generating a blue-colored product [36]. To evaluate the •OH generation, TA was utilized. As a •OH specific probe, TA could easily bind with •OH and generate the fluorescent 2-hydroxyl terephthalic acid (Fig. 6A). As shown in Fig. 6B, strong fluorescence was obtained for the solution

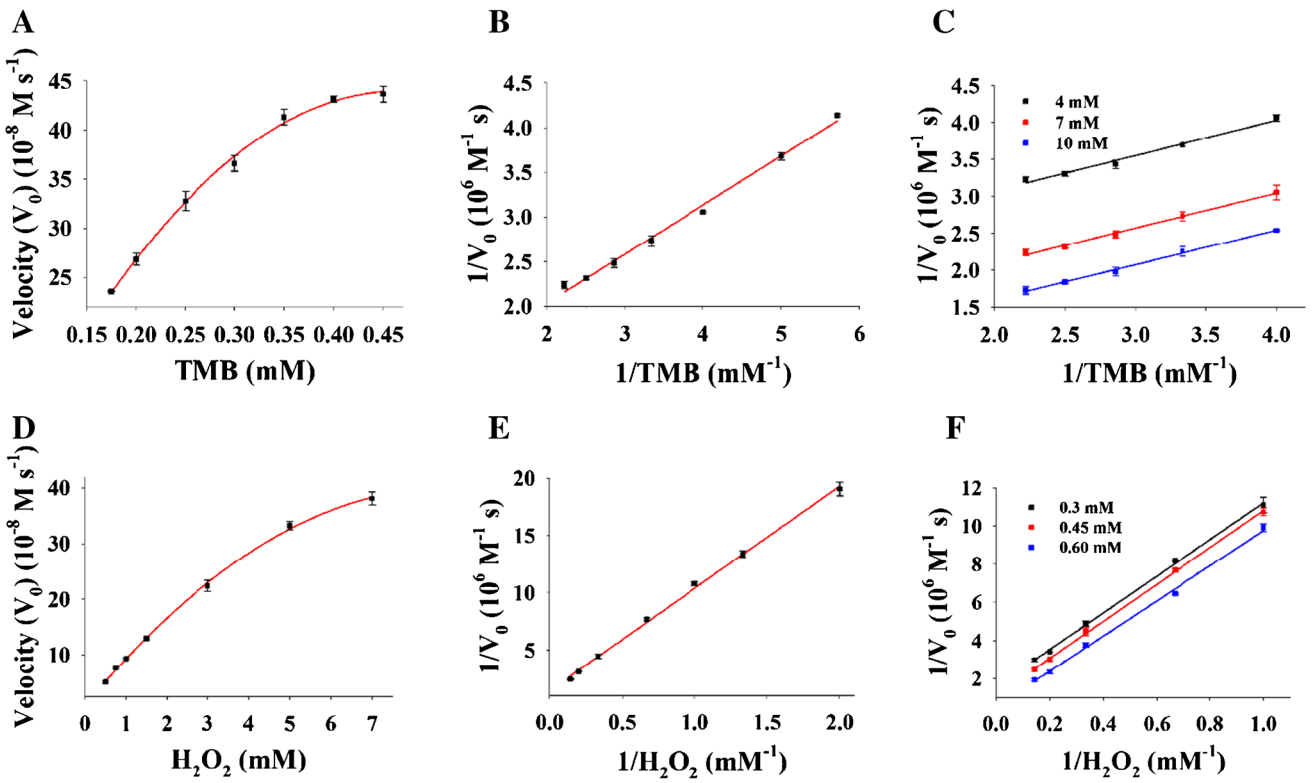

Fig. 5 Steady-state kinetic assays of the MPNs for TMB oxidation in the presence of H_2O_2. **A**, **D** Michaelis–Menten and **B**, **E** Lineweaver–Burk plots for TMB and H_2O_2. The concentrations of TMB and H_2O_2 were fixed at 0.45 mM and 7.0 mM, respectively. **C**, **F** Lineweaver–Burk plots for various substrate concentrations

Table 1 A comparison of the kinetic parameters of the MPNs and various Pt-based catalysts

Catalyst	Substrate	K_m (mM)	$V_{max} \times 10^{-8}$ (M s^{-1})	k_{cat} (s^{-1})	Ref
HRP	TMB	0.434	10.00	4.00×10^3	[2]
	H_2O_2	3.70	8.71	3.48×10^3	
ISPtNPs	TMB	0.120	126	2.27×10^4	[32]
	H_2O_2	769	185	1.55×10^4	
uPtNZs	TMB	0.174	101	2.69×10^4	[33]
	H_2O_2	82.7	177	4.75×10^4	
PtHND	TMB	0.81	12.0	1.70×10^{-2}	[34]
	H_2O_2	6.90	9.90	1.40×10^{-2}	
Pd@Pt NPs	TMB	1.78	36.4	1.42×10^{-2}	[35]
	H_2O_2	0.053	9.26	0.36×10^{-2}	
MPN	TMB	0.570	104.9	4.87×10^6	This work
	H_2O_2	5.81	65.4	3.04×10^6	

ISPtNPs, irregular-shaped Pt nanoparticles; *uPtNZs*, urchin-like Pt nanozymes; *PtHND*, Pt hollow nanodendrite

which contains TA, MPNs, and H_2O_2, while fluorescence was negligible in the absence of MPNs or H_2O_2. Moreover, the fluorescence signal significantly decreased for solutions containing DMSO, which scavenges •OH. Consequently, these results demonstrate that the •OH species was generated from H_2O_2 decomposition by the MPNs as peroxidase-like nanozymes.

As the active species are generated in the catalytic process, electron transfer between the MPNs and substrates can take place. To evaluate the electron transfer, the electrochemical measurements for the redox reaction of H_2O_2 was conducted using cyclic voltammetry (CV) and chronoamperometry (CA). An ITO glass was modified with the MPNs and Nafion and used as a working electrode (Nafion/MPN/ITO) in the electrochemical experiments. Figure 6C shows the CV responses of Nafion/MPN/ITO in the absence or presence of the H_2O_2. In the absence of H_2O_2, a weak current was observed while an obvious reduction peak at around − 0.79 V (vs Ag/AgCl) was observed in the presence of H_2O_2. Based on the CV results, the amperometric response to the continuous addition of H_2O_2 was recorded at a reduction potential of − 0.79 V (Fig. 6D). The reduction current increased after the addition of H_2O_2 and reached a steady-state value within a few seconds. The current response of Nafion/MPN/ITO for H_2O_2 was higher than that of Nafion/ITO, suggesting the nanozyme-catalyzed electron transfer between the electron donor (electrode)

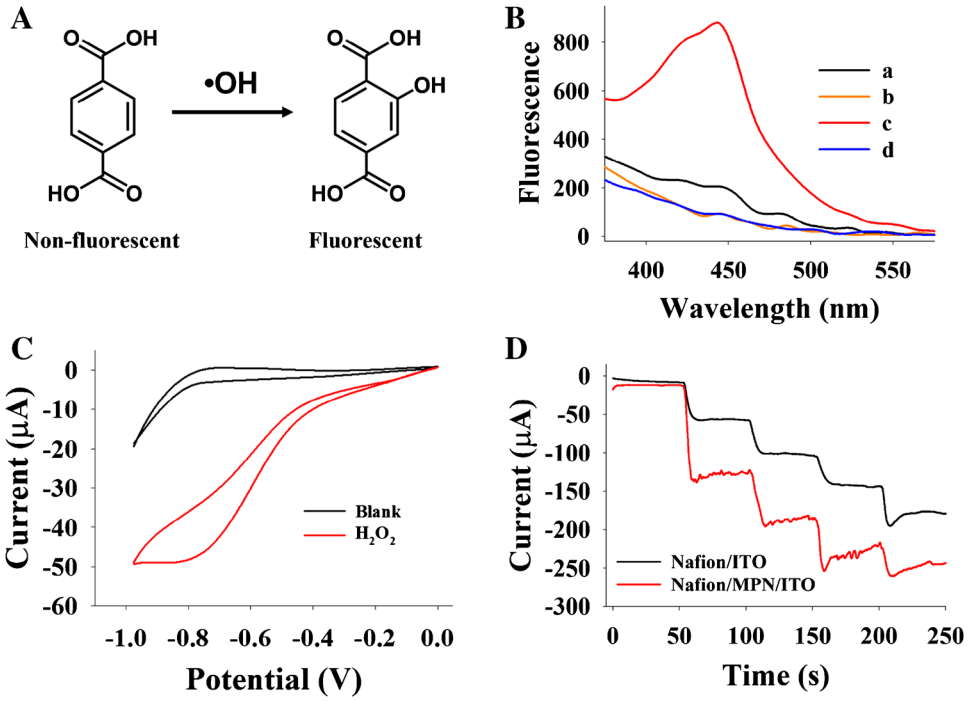

Fig. 6 **A** Reaction mechanism of terephthalic acid (TA) with hydroxyl radical (•OH). **B** Fluorescence spectra of various compositions: (a) TA + H_2O_2, (b) TA + MPNs, (c) TA + H_2O_2 + MPNs, and (d) TA + H_2O_2 + MPNs + DMSO. **C** Cyclic voltammetry of a Nafion/MPN/ITO electrode in PBS (10 mM) in the presence and absence of H_2O_2 at a scan rate of 50 mV/s. **D** The chrono-amperometric current responses of Nafion/ITO (black line) and Nafion/MPN/ITO (red line) for the continuous addition of H_2O_2 (1 M) every 50 s at a fixed potential of − 0.79 V

and acceptor (H_2O_2). Consequently, these results suggest that the electron transfer can be realized and enhanced with the aid of the MPNs.

Surface modification of the MPNs

To obtain the dAb-CRP/MPN complex, the carboxyl group (-COOH) was modified on the surface of the MPNs. As Pt can bind with thiol [37, 38], the surface of the MPNs can be easily modified with -COOH through the PEGylation of thiolated carboxylic PEG (HS-PEG_{3500}-COOH) chains. The immobilized -COOH could serve as a reactive site to bind the antibodies. The immobilization of HS-PEG_{3500}-COOH was confirmed by Ellman's test (Fig. S5). As HS-PEG_{3500}-COOH is immobilized on the MPNs, the concentration of HS-PEG_{3500}-COOH in the supernatant decreases, which results in a decrease of the absorbance signal produced from the reaction between Ellman's reagent and HS-PEG_{3500}-COOH. After 4 h reaction between the MPNs and HS-PEG_{3500}-COOH, the absorbance of Ellman's reagent for the supernatant was significantly decreased compared to the added concentration (Table S1). The concentration of HS-PEG_{3500}-COOH for the supernatant calculated from the calibration curve was about 0.34 μM, indicating that almost 99% of 25 μM HS-PEG_{3500}-COOH reacted with the MPNs. These results demonstrate successful modification of HS-PEG_{3500}-COOH on the surface of the MPNs.

ELISA for CRP

The carboxylated MPNs were modified with anti-CRP detection antibody (dAb-CRP) through the EDC/NHS coupling reaction. After modification of the dAb-CRP on the MPNs, the catalytic activity decreased about 20% due to the blocking the active site of the MPNs by dAb-CRP (Fig. S6). Although the catalytic activity decreased, the dAb-CRP-modified MPNs preserved enough peroxidase-like activity for CRP detection. Then, the dAb-CRP-modified MPNs were applied for CRP ELISA. The MPN-based ELISA is systemically the same as HRP-based ELISA except that the MPNs are replaced with HRP (Fig. 7A). The procedures and the CRP standard concentrations of both ELISAs were kept the same to allow an accurate comparison. The 96-well plate, which was immobilized by anti-CRP capture antibody (cAb-CRP), was treated with CRP concentrations (0–7.8 ng/mL), followed by the treatment of dAb-CRP/MPN or HRP-anti-CRP antibodies. In this way, each well possesses different concentrations of dAb-CRP/MPN or HRP-anti-CRP antibodies. After the addition of TMB/H_2O_2 solutions to each well, blue-colored products (TMB_{ox}) were generated with different intensities. Then, the stop solution (0.5 M H_2SO_4) was added and the yellow-colored products were monitored in the 96-well plate (Fig. 7B). Finally, the absorbance was recorded. The developed MPN-based ELISA for CRP detection showed linearity in the range of 0.24 to 7.8 ng/mL with a correlation coefficient (R^2) of 0.992. Furthermore, the limit of detection (LOD) was calculated to be 0.13 ng/

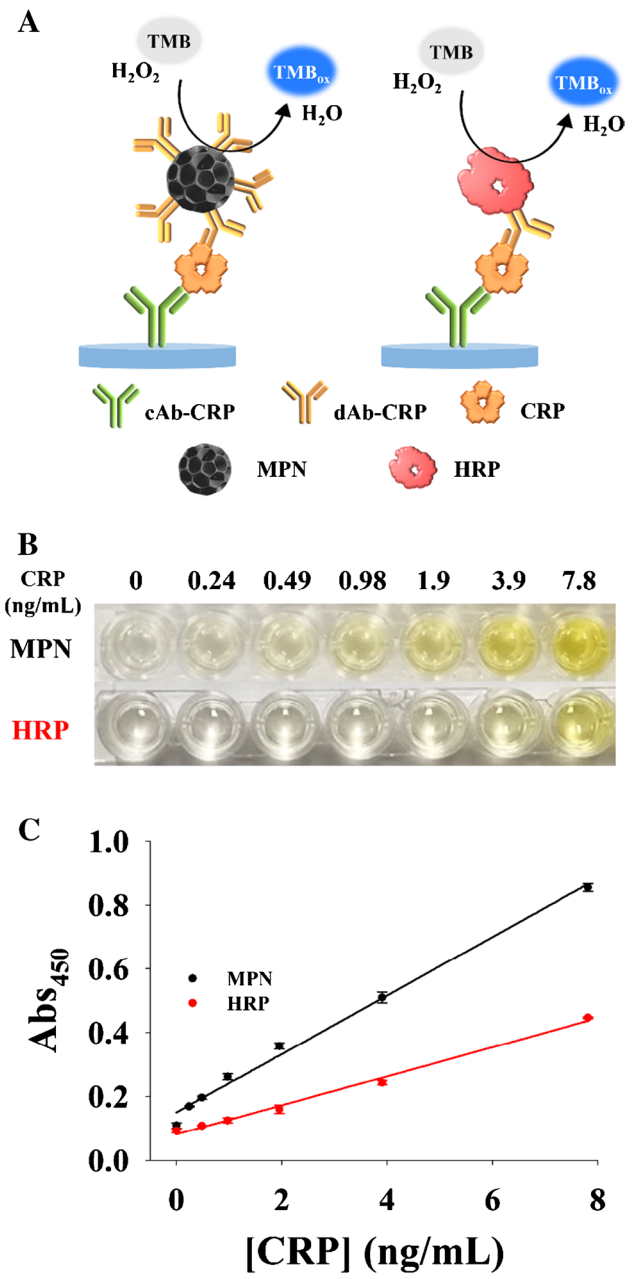

Fig. 7 **A** Schematic illustration of MPN-based ELISA and conventional HRP-based ELISA for CRP detection. **B** Optical image of MPN-based ELISA and HRP-based ELISA for CRP detection. **C** Calibration curves for CRP concentrations using MPN (black line) or HRP (red line) ELISA

mL (Fig. 7C). In contrast, conventional HRP-based ELISA shows a linear detection range from 0.49 to 7.8 ng/mL with a LOD of 0.35 ng/mL and R^2 of 0.995. The LOD was obtained by dividing the three standard deviations of the blank sample by the slope of the calibration curve. When comparing the LOD and slope values of the calibration curves under the same CRP concentration ranges, MPN-based ELISA was more sensitive than HRP-based ELISA. These

Table 2 A comparison of analytical performance of the MPN-based ELISA and other analytical methods

Materials	Method	Detection range (ng/mL)	LOD (ng/mL)	Ref
Au-MOF	Electro-chemical	1–400	0.2	[39]
MB, HRP	Electro-chemical	2–100	0.47	[40]
CdSe/ZnS QDs	Fluorescence	1.56–400	0.46	[41]
Ag NPs	SERRS	1.5–25	1.0	[42]
MPNs	Colorimetric	0.24–7.8	0.13	This work

MB, magnetic beads; *HRP*, horseradish peroxidase; *SERRS*, surface enhanced resonance Raman scattering

enhanced detection sensitivities of MPN-based ELISA could be ascribed to the higher catalytic efficiency of the MPNs compared to HRP. Furthermore, the analytical performance of MPN-based ELISA was compared with other methods (Table 2). The other methods showed good analytical performance with broad detection range. However, those methods still reveal some limitations such as sophisticated equipment and complicated operation. In contrast, although the MPN-based colorimetric method has narrow detection range, this method shows many advantages including simplicity of manipulations, low cost, and high sensitivity.

Then, the impact on potential interferences such as human serum albumin (HSA), glucose, AA, urea, uric acid (UA), and creatinine (CT) was investigated. The concentration of interferences was chosen according to their physiological level in serum: HSA (50 mg/mL), glucose (1 mg/mL), AA (6 ug/mL), urea (200 ug/mL), UA (80 ug/mL), and CT (12 ug/mL). Each interference was mixed with CRP standard sample (7.8 ng/mL) and analyzed using MPN-based ELISA. As shown in Fig. S7, the potential interferences showed negligible fluctuations of less than 10% compared to the sample containing only CRP standard. This result demonstrates that the MPN-based ELISA has excellent specificity for the detection of CRP.

Recovery test

For the recovery test, CRP samples (1 and 5 ng/mL) were prepared by adding CRP to human serum. Table S2 shows the recoveries of the spiked CRP using MPN-based ELISA. The observed recovery values of 1 and 5 ng/mL CRP were 98.6% and 102%, and relative standard deviations were 8.63% and 2.18%, respectively. The above results reveal the applicability and effectiveness of the MPN-based ELISA for sensitive and accurate detection of CRP in real samples.

Conclusions

In summary, MPNs prepared by a simple synthetic method displayed enhanced peroxidase-like activity due to the presence of a mesoporous network, which increases the surface to volume ratio. As a peroxidase-like nanozyme, the MPNs followed Michaelis–Menten kinetics with splendid catalytic efficiency for TMB and H_2O_2. Moreover, the MPNs exhibited typical ping-pong kinetics. Further studies demonstrated that the catalytic mechanism of the MPNs was based on the decomposition of H_2O_2 and generation of •OH. The MPNs were modified with dAb-CRP using EDC/NHS coupling and then applied to CRP detection. The MPN-based ELISA displayed sensitive detection of CRP in a concentration range from 0.24 to 7.8 ng/mL with a LOD of 0.13 ng/mL, which is more sensitive than HRP-based ELISA. Moreover, MPN-based ELISA can recover CRP from spiked human serum samples. Due to the several advantages such as simple production, great stability, and excellent enzyme-like activity, we believe that the MPNs can be applied to a wide range of fields.

Supplementary Information The online version contains supplementary material available at https://doi.org/10.1007/s00216-022-04271-5.

Author contribution SES: conceptualization, methodology, investigation, formal analysis, visualization, writing — original draft. PKG: investigation. WH: investigation. HBL: investigation. YP: investigation. JP: investigation. SNK: investigation. GHS: supervision, visualization, writing — review and editing, funding acquisition.

Funding This research was supported by the Basic Science Research Program through the National Research Foundation (NRF) of Korea (2018R1A6A1A03024231 and 2021R1A2C1003566).

Declarations

Conflict of interest The authors declare no competing interests.

References

1. Huang Y, Ren J, Qu X. Nanozymes: classification, catalytic mechanisms, activity regulation, and applications. Chem Rev. 2019;119(6):4357–412.
2. Gao LZ, Zhuang J, Nie L, Zhang JB, Zhang Y, Gu N, et al. Intrinsic peroxidase-like activity of ferromagnetic nanoparticles. Nat Nanotechnol. 2007;2(9):577–83.
3. Son SE, Gupta PK, Hur W, Lee HB, Park Y, Park JY, et al. Citric acid-functionalized rhodium-platinum nanoparticles as peroxidase mimics for determination of cholesterol. Acs Appl Nano Mater. 2021;4(8):8282–91.
4. Son SE, Ko E, Tran VK, Hur W, Choi H, Lee HB, et al. Highly sensitive electrochemical determination of norepinephrine using poly acrylic acid-coated nanoceria. ChemElectroChem. 2019;6(17):4666–73.
5. Kim MS, Cho S, Joo SH, Lee J, Kwak SK, Kim MI, et al. N- and B-codoped graphene: a strong candidate to replace natural peroxidase in sensitive and selective bioassays. ACS Nano. 2019;13(4):4312–21.
6. Christus AAB, Ravikumar A, Panneerselvam P, Radhakrishnan K. A novel Hg(II) sensor based on Fe3O4@ZnO nanocomposite as peroxidase mimics. Appl Surf Sci. 2018;449:669–76.
7. He YF, Niu XH, Li LH, Li X, Zhang WC, Zhao HL, et al. Microwave-assisted fabrication of bimetallic PdCu nanocorals with enhanced peroxidase-like activity and efficiency for thiocyanate sensing. Acs Appl Nano Mater. 2018;1(5):2397–405.
8. Hashmi S, Singh M, Weerathunge P, Mayes ELH, Mariathomas PD, Prasad SN, et al. Cobalt sulfide nanosheets as peroxidase mimics for colorimetric detection of L-cysteine. Acs Appl Nano Mater. 2021;4(12):13352–62.
9. Wang J, Hu Y, Zhou Q, Hu L, Fu W, Wang Y. Peroxidase-like activity of metal-organic framework [Cu(PDA)(DMF)] and its application for colorimetric detection of dopamine. ACS Appl Mater Interfaces. 2019;11(47):44466–73.
10. Cheng Q, Yang Y, Peng Y, Liu M. Pt nanoparticles with high oxidase-like activity and reusability for detection of ascorbic acid. Nanomaterials (Basel). 2020;10(6):1015.
11. Gupta PK, Son SE, Seong GH. Functionalized ultra-fine bimetallic PtRu alloy nanoparticle with high peroxidase-mimicking activity for rapid and sensitive colorimetric quantification of C-reactive protein. Mikrochim Acta. 2021;188(4):119.
12. You JG, Liu YW, Lu CY, Tseng WL, Yu CJ. Colorimetric assay of heparin in plasma based on the inhibition of oxidase-like activity of citrate-capped platinum nanoparticles. Biosens Bioelectron. 2017;92:442–8.
13. Wu LL, Wang LY, Xie ZJ, Pan N, Peng CF. Colorimetric assay of L-cysteine based on peroxidase-mimicking DNA-Ag/Pt nanoclusters. Sensor Actuat B-Chem. 2016;235:110–6.
14. Bian B, Zhu XX, Wu Q, Liu Y, Liu SW, Liu QY, et al. Pt and ZnFe2O4 nanoparticles immobilized on carbon for the detection of glutathione. Acs Appl Nano Mater. 2021;4(9):9479–88.
15. Chen PK, Lai NC, Ho CH, Hu YW, Lee JF, Yang CM. New synthesis of MCM-48 nanospheres and facile replication to mesoporous platinum nanospheres as highly active electrocatalysts for the oxygen reduction reaction. Chem Mater. 2013;25(21):4269–77.
16. Attard GS, Goltner CG, Corker JM, Henke S, Templer RH. Liquid-crystal templates for nanostructured metals. Angew Chem Int Edit. 1997;36(12):1315–7.
17. Wang HJ, Jeong HY, Imura M, Wang L, Radhakrishnan L, Fujita N, et al. Shape- and size-controlled synthesis in hard templates: sophisticated chemical reduction for mesoporous monocrystalline platinum nanoparticles. J Am Chem Soc. 2011;133(37):14526–9.
18. Baba D, Kim J, Henzie J, Li CL, Jiang B, Dag O, et al. Electrochemical deposition of large-sized mesoporous nickel films using polymeric micelles. Chem Commun. 2018;54(73):10347–50.
19. Wang N, Xu Y, Han Y, Gao CZ, Cao X. Mesoporous Pd@M (M = Pt, Au) microrods as excellent electrocatalysts for methanol oxidation. Nano Energy. 2015;17:111–9.
20. Xie YD, Kocaefe D, Chen CY, Kocaefe Y. Review of research on template methods in preparation of nanomaterials. J Nanomater. 2016;2016:2302595.
21. Li C, Iqbal M, Jiang B, Wang Z, Kim J, Nanjundan AK, et al. Pore-tuning to boost the electrocatalytic activity of polymeric micelle-templated mesoporous Pd nanoparticles. Chem Sci. 2019;10(14):4054–61.
22. Jiang B, Li C, Dag O, Abe H, Takei T, Imai T, et al. Mesoporous metallic rhodium nanoparticles. Nat Commun. 2017;8:15581.
23. Jiang B, Li C, Tang J, Takei T, Kim JH, Ide Y, et al. Tunable-sized polymeric micelles and their assembly for the preparation of large mesoporous platinum nanoparticles. Angew Chem Int Ed Engl. 2016;55(34):10037–41.

24. Sproston NR, Ashworth JJ. Role of C-reactive protein at sites of inflammation and infection. Front Immunol. 2018;9:754.
25. Emerging Risk Factors C, Kaptoge S, Di Angelantonio E, Lowe G, Pepys MB, Thompson SG, et al. C-reactive protein concentration and risk of coronary heart disease, stroke, and mortality: an individual participant meta-analysis. Lancet. 2010;375(9709):132–140.
26. Jiang B, Li C, Malgras V, Imura M, Tominaka S, Yamauchi Y. Mesoporous Pt nanospheres with designed pore surface as highly active electrocatalyst. Chem Sci. 2016;7(2):1575–81.
27. Liu Y, Fu S, Lin L, Cao Y, Xie X, Yu H, et al. Redox-sensitive Pluronic F127-tocopherol micelles: synthesis, characterization, and cytotoxicity evaluation. Int J Nanomedicine. 2017;12:2635–44.
28. Jiang B, Li CL, Malgras V, Imura M, Tominakaa S, Yamauchi Y. Mesoporous Pt nanospheres with designed pore surface as highly active electrocatalyst. Chem Sci. 2016;7(2):1575–81.
29. Gupta PK, Pachauri N, Khan ZH, Solanki PR. One pot synthesized zirconia nanoparticles embedded in amino functionalized amorphous carbon for electrochemical immunosensor. J Electroanal Chem. 2017;807:59–69.
30. Yang MZ, Guan YP, Yang Y, Xia TT, Xiong WB, Wang N, et al. Peroxidase-like activity of amino-functionalized magnetic nanoparticles and their applications in immunoassay. J Colloid Interf Sci. 2013;405:291–5.
31. Porter DJ, Bright HJ. The mechanism of oxidation of nitroalkanes by horseradish peroxidase. J Biol Chem. 1983;258(16):9913–24.
32. Gao ZQ, Xu MD, Hou L, Chen GN, Tang DP. Irregular-shaped platinum nanoparticles as peroxidase mimics for highly efficient colorimetric immunoassay. Anal Chim Acta. 2013;776:79–86.
33. Choi H, Son SE, Hur W, Tran V-K, Lee Han B, Park Y, et al. Electrochemical immunoassay for determination of glycated albumin using nanozymes. Sci Rep-Uk. 2020;10(1):9513.
34. Wu RF, Chong Y, Fang G, Jiang XM, Pan Y, Chen CY, et al. Synthesis of Pt hollow nanodendrites with enhanced peroxidase-like activity against bacterial infections: implication for wound healing. Adv Funct Mater. 2018;28(28):1801484.
35. Jiang T, Song Y, Du D, Liu XT, Lin YH. Detection of p53 protein based on mesoporous Pt-Pd nanoparticles with enhanced peroxidase-like catalysis. Acs Sensors. 2016;1(6):717–24.
36. Gao Z, Hou L, Xu M, Tang D. Enhanced colorimetric immunoassay accompanying with enzyme cascade amplification strategy for ultrasensitive detection of low-abundance protein. Sci Rep. 2014;4:3966.
37. Vericat C, Vela ME, Corthey G, Pensa E, Cortes E, Fonticelli MH, et al. Self-assembled monolayers of thiolates on metals: a review article on sulfur-metal chemistry and surface structures. Rsc Adv. 2014;4(53):27730–54.
38. Yang BW, Agrios AG. Attachment of Pt nanoparticles to a metal oxide surface using a thiol-carboxyl bifunctional molecule. J Colloid Interf Sci. 2018;513:464–9.
39. Liu TZ, Hu R, Zhang X, Zhang KL, Liu Y, Zhang XB, et al. Metal-organic framework nanomaterials as novel signal probes for electron transfer mediated ultrasensitive electrochemical immunoassay. Anal Chem. 2016;88(24):12516–23.
40. de Avila BEF, Escamilla-Gomez V, Lanzone V, Campuzano S, Pedrero M, Compagnone D, et al. Multiplexed determination of amino-terminal pro-B-type natriuretic peptide and C-reactive protein cardiac biomarkers in human serum at a disposable electrochemical magnetoimmunosensor. Electroanal. 2014;26(2):254–61.
41. Lv YB, Wu RL, Feng KR, Li JJ, Mao Q, Yuan H, et al. Highly sensitive and accurate detection of C-reactive protein by CdSe/ZnS quantum dot-based fluorescence-linked immunosorbent assay. J Nanobiotechnol. 2017;15(1):35.
42. Sloan-Dennison S, Laing S, Shand NC, Graham D, Faulds K. A novel nanozyme assay utilising the catalytic activity of silver nanoparticles and SERRS. Analyst. 2017;142(13):2484–90.